Guiding fields for phase separation: Controlling Liesegang patterns

T. Antal,[1] I. Bena,[2] M. Droz,[2] K. Martens,[2] and Z. Rácz[3]
[1]*Program for Evolutionary Dynamics, Harvard University, Cambridge, Massachusetts 02138, USA*
[2]*Theoretical Physics Department, University of Geneva, CH-1211 Geneva 4, Switzerland*
[3]*Institute for Theoretical Physics–HAS, Eötvös University, Pázmány sétány 1/a, 1117 Budapest, Hungary*
(Received 5 June 2007; published 3 October 2007)

Liesegang patterns emerge from precipitation processes and may be used to build bulk structures at submicrometer length scales. Thus they have significant potential for technological applications provided adequate methods of control can be devised. Here we describe a simple, physically realizable pattern control based on the notion of *driven precipitation*, meaning that the phase separation is governed by a guiding field such as, for example, a temperature or pH field. The phase separation is modeled through a nonautonomous Cahn-Hilliard equation whose spinodal is determined by the evolving guiding field. Control over the dynamics of the spinodal gives control over the velocity of the instability front that separates the stable and unstable regions of the system. Since the wavelength of the pattern is largely determined by this velocity, the distance between successive precipitation bands becomes controllable. We demonstrate the above ideas by numerical studies of a one-dimensional system with a diffusive guiding field. We find that the results can be accurately described by employing a linear stability analysis (pulled-front theory) for determining the velocity–local-wavelength relationship. From the perspective of the Liesegang theory, our results indicate that the so-called revert patterns may be naturally generated by diffusive guiding fields.

DOI: 10.1103/PhysRevE.76.046203 PACS number(s): 05.70.Ln, 64.60.My, 85.40.Hp, 82.20.−w

I. INTRODUCTION

Pattern formation is a ubiquitous phenomenon in out-of-equilibrium systems, and ordered structures often emerge in the wake of a moving reaction front [1]. There has been increasing interest recently, both experimental and theoretical, in the study of various types of chemically generated patterns. The main reason is that they are expected to provide new bottom-up, self-assembling technologies for engineering bulk patterns on mesoscopic and microscopic scales (for illustration, see, e.g., [2–7] from a rapidly growing bibliography), for which the traditional top-down methods (i.e., removing material in order to create a structure) are reaching the limits of their capabilities.

Detailed understanding of the mechanisms responsible for pattern formation is a key element in developing technological applications since it helps in constructing the appropriate tools for the control of the characteristics of the emerging patterns. In this paper we shall focus on designing a simple method to control the so-called Liesegang structures [8,9]. In particular, this method should be useful for a recently proposed experimental setup that allows one to create stamps of such structures [4].

Depending on the geometry, Liesegang precipitation patterns are bands (in an axially symmetric configuration), rings (in a circular), or shells (in a spherically symmetric configuration), clearly separated in the direction of motion of a chemical reaction front. Several generic experimental laws characterize the patterns (see, e.g., [10,11] for reviews). In particular, it is found that the positions of the bands usually obey simple laws; e.g., they form, with a good approximation, a geometric series with increasing distance between consecutive bands. This is the so-called regular banding situation, which has been recently explained [12] using the phase separation in the presence of a moving front as the underlying mechanism. Briefly, the reaction front, which moves diffusively, leaves behind a constant concentration c_0 of the reaction product, which we shall conventionally name hereafter C particles [13–15]. At a coarse-grained level, the dynamics of the C particles (which can diffuse, and are also attracting each other) can be described by a Cahn-Hilliard (CH) equation [16–18] with a source term corresponding to the moving reaction front. Starting with a system free of C's, the dynamics of the front locally brings the system across the spinodal line, provided that c_0 is inside the unstable region of the phase diagram. A phase separation then takes place on a short time scale, and a band of precipitate is rapidly formed just behind the front. This band acts as a sink for the C particles. Then the local concentration of C's decreases, bringing the system locally into the stable phase again. Thus Liesegang patterns are formed, since the state of the system at the front is locally and quasiperiodically driven into the unstable regime.

The characteristics of these regular patterns can be controlled to some extent through an appropriate choice of the concentration of the reagents [19], of the nature of the gel that is filling the reaction container [20], of the shape of the container [5], or through an applied electric field [21–24].

The spinodal decomposition scenario has proved its power by describing regular patterns and, furthermore, by explaining how those patterns can be influenced by the concentration of the outer and inner electrolytes and by an external electric field. We will show that it can be extended to describe other situations, as well. Indeed, there is experimental evidence of Liesegang-type precipitation patterns with decreasing distances between successive bands [25], which is termed inverse banding. In the borderline case between regular and inverse banding, the distances between successive bands are constant, a situation called equidistant banding [26]. In our attempts at describing the above patterns we were led to a mechanism that may provide a simple, experi-

mentally realizable control tool of the emerging pattern.

As described in detail in Sec. II, our proposal is based on a phase separation mechanism in a space- and time-dependent guiding field, which could represent, for example, a temperature or pH field. The pattern formation is thus modeled through a nonautonomous CH equation, whose spinodal line is controlled by the guiding field. Note that the present design of the guiding field is different from the homogeneous (overall) cooling that was used in most of the previous studies of nonautonomous CH models (see, e.g., [27–30]). As we shall demonstrate, a simple guiding field is sufficient to generate crossover between regular and inverse patterns. For example, such a guiding field can be a temperature field evolving diffusively due to a temperature difference at the boundaries of the system, whose characteristics are detailed in Sec. III. The features of the corresponding emerging patterns are analyzed in Sec. IV. As discussed in Sec. V, our numerical findings can be justified by theoretical arguments relating the velocity of the front of the guiding field to the pulled-front velocity resulting from a linear stability analysis of the phase separation process. Other, more flexible ways to control the patterns are also briefly presented in Sec. VI. Finally, conclusions and perspectives are discussed in Sec. VII.

II. THE MODEL

Let us consider a tube filled with gel, and an initially uniform concentration c_0 of C particles throughout the tube. Assuming axial symmetry along the x axis of the tube, we shall consider that the C-particle concentration $c(x,t)$ evolves in time according to the Cahn-Hilliard equation in one dimension. After rescaling the space and time variables, this equation can be written in the following dimensionless form:

$$\frac{\partial c(x,t)}{\partial t} = -\frac{\partial^2}{\partial x^2}\left(\varepsilon c(x,t) - c^3(x,t) + \frac{\partial^2 c(x,t)}{\partial x^2}\right), \tag{1}$$

with $0 \leqslant x \leqslant L$, where L is the dimensionless length of the tube. Note that we also performed an appropriate shift and scaling of the concentration that allows us to write the CH equation in a form that is more convenient for the exposition of our problem; namely, this form is symmetric with respect to the change in sign of c, $c \leftrightarrow -c$ (see, e.g., [10,12] and [32] for a more detailed discussion of this point). The shifted and rescaled concentration can take both positive and negative values, and the stable configurations are symmetric around $c=0$.

The parameter ε measures the deviation of the temperature from the critical temperature T_c; it is negative for temperatures above T_c (for which no phase separation is possible), while it is positive for temperatures $T<T_c$. Below the critical temperature, a uniform concentration profile c_0 inside the spinodal decomposition domain, i.e., $|c_0| \leqslant c_s = \sqrt{\varepsilon/3}$, is linearly unstable. A small, localized perturbation of the concentration can then trigger a phase separation throughout the system, through the amplification of the unstable modes of wave numbers $|k| < \sqrt{\varepsilon}$. A large body of work (see, e.g., [31]) has been devoted to the study of the phase separation process in the simple case of a uniform parameter ε taking the same value throughout the system.

Here we shall concentrate on a different situation, namely, when ε is a field, which evolves according to its own dynamics. Moreover, it is possible to control its evolution. For a simple realization of this control consider the following situation. Suppose that at a time $t=0$ the temperature at one end of the tube is lowered and kept at a constant value $T_0 < T_c$ thereafter. The other end of the tube is supposed to be thermally isolated [33]. The temperature profile then evolves in time along the tube according to the usual Fourier law of heat conduction, and so does the related $\varepsilon(x,t)$ field,

$$\frac{\partial \varepsilon(x,t)}{\partial t} = D\frac{\partial^2 \varepsilon(x,t)}{\partial x^2}, \tag{2}$$

where D is the dimensionless thermal diffusion coefficient. Through an appropriate scaling of the temperature, the value of ε can be set to -1 throughout the system at $t=0$, while $\varepsilon=+1$ at $t \geqslant 0$ at the left ($x=0$) end of the tube; at the right ($x=L$) end of the tube there is no heat flow:

$$\varepsilon(x>0, t=0) = -1,$$

$$\varepsilon(x=0,t) = +1,$$

$$\frac{\partial \varepsilon}{\partial x}(x=L,t) = 0. \tag{3}$$

These equations (2) and (3) define completely the evolution of $\varepsilon(x,t)$ along the tube, from the onset of the cooling procedure until the asymptotic uniform profile $\varepsilon=+1$ is reached throughout the tube [32].

For the value $\varepsilon=-1$, the uniform concentration profile c_0 is stable, while for $\varepsilon=+1$ it tends to phase separate (i.e., the initial concentration $|c_0| < \sqrt{1/3}$). Therefore, with the advancing cooling front, the C-particle concentration becomes locally unstable with respect to phase separation. As a consequence, a pattern made of alternating low- and high-density phases of C appears simultaneously to the propagation of the cooling front along the tube. Its properties and characteristics result thus from the CH equation (1) coupled to the evolution equation (2) for $\varepsilon(x,t)$. Appropriate boundary conditions (i) guarantee the conservation of C particles inside the tube (more precisely, zero particle fluxes J_c at the edges), and (ii) associated with the initial condition, also ensure the uniqueness of the solution. The boundary conditions we used in our numerical discretized procedure amount, in the continuum limit, to

$$J_c(x=0 \text{ and } L, t) = 0,$$

$$\frac{\partial^3 c}{\partial x^3}(x=0 \text{ and } L, t) = 0, \tag{4}$$

with $J_c(x,t) = \partial(\varepsilon c - c^3 + \partial^2 c/\partial x^2)/\partial x$. Setting $\partial^3 c/\partial x^3 = 0$ means that c at the boundaries relaxes to $c = \pm\sqrt{\varepsilon}$ determined by the boundary value of ε. More detailed considerations, including other types of boundary conditions and appropriate

discretization schemes, are discussed, e.g., in Refs. [34].

The field $\varepsilon(x,t)$ related to the diffusive temperature profile is thus playing the role of a guiding field. One can think, however, of other types of fields $\varepsilon(x,t)$, and other boundary and initial conditions for an experimental setup. As an example, one can assume that a chemical agent is diffusing from one reservoir at the $x=0$ end of the tube; its concentration changes the local pH of the system, and thus may drive the C particles to phase separation, etc. Accordingly, we hereafter call ε the guiding field, and thus do not restrict ourselves to the temperaturelike interpretation.

III. CHARACTERISTICS OF THE DIFFUSIVE GUIDING FIELD $\varepsilon(x,t)$

During its time evolution, the guiding field $\varepsilon(x,t)$ will locally modify the position of the spinodal line. At a fixed time t, the spinodal density $c_s=\sqrt{\varepsilon(x,t)/3}$ will reach the value $|c_0|$ at a given point $x_f=x_f(t)$, therefore initiating a phase separation locally. The point $x_f(t)$ defines the position of the instability front, which is thus determined by the condition $\varepsilon(x=x_f,t)=3c_0^2$. Behind the front, which propagates to the right, the system becomes locally unstable, and phase separates into a precipitation pattern of alternate high- and low-density regions of C.

The diffusion equation (2) for $\varepsilon(x,t)$ with the prescribed boundary and initial conditions (3) can be solved through a simple Laplace transform method [35]. One obtains for x_f an implicit equation comprising an infinite sum,

$$\sum_{n=0}^{\infty} \frac{(-1)^n}{2n+1} \exp\left[-\frac{(2n+1)^2\pi^2}{4}\left(\frac{tD}{L^2}\right)\right] \times \cos\left[\frac{(2n+1)\pi}{2}\left(1-\frac{x_f}{L}\right)\right] = \frac{\pi(1+3c_0^2)}{8}. \quad (5)$$

The resulting trajectory of the instability front $x_f(t)$, as well as its velocity $v_f(t)=dx_f(t)/dt$ for a particular choice of c_0 are represented in Fig. 1. Note that, when the spatial, temporal, and velocity variables are rescaled, respectively, by L, L^2/D, and D/L, as indicated on the axis of these plots, the curves for the trajectory and velocity of the instability front are universal (for a given value of c_0).

As can be seen in Fig. 1, the front moves diffusively at the beginning, and it accelerates past a crossover point P where the acceleration is zero. The large-time asymptote for the front position can be obtained by keeping only the leading $n=0$ term in the sum (5),

$$x_f(t) \approx L\left\{1-\frac{2}{\pi}\arccos\left[\frac{\pi(1+3c_0^2)}{8}\exp\left(\frac{\pi^2 Dt}{4L^2}\right)\right]\right\}. \quad (6)$$

This approximate expression is valid provided $L^2/2\pi^2 D = t_{\min} \lesssim t \lesssim t_{\max} = (4L^2/\pi^2 D)\ln\{8/[\pi(1+3c_0^2)]\}$ where $t_{\min}$ is the time when the $n=1$ term in the sum (5) becomes negligible with respect to the $n=0$ term, while $t_{\max}$ represents a rough estimate of the time it takes the instability front to reach the end ($x=L$) of the tube. The function given by Eq. (6) is shown in the upper panel of Fig. 1, and one can see

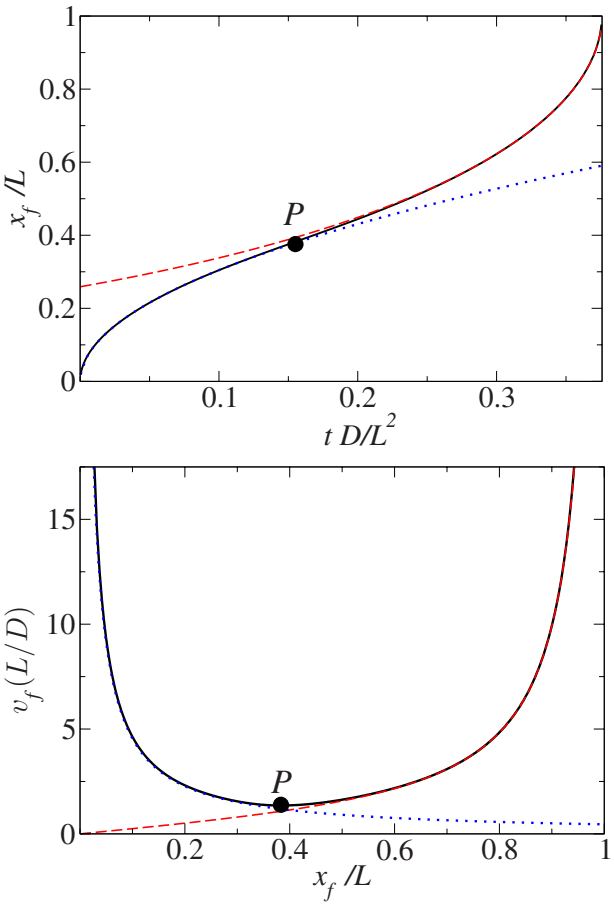

FIG. 1. (Color online) Upper panel: Time evolution of the front position for $c_0=-0.05$ (solid line). The front moves diffusively for small t, $x_f(t)\sim\sqrt{t}$ (dotted line), while the large-time asymptote is given by Eq. (6) (dashed line). Lower panel: The velocity of the instability front v_f as a function of the front position x_f (solid line). The short-time asymptote $v_f(t)\sim 1/\sqrt{t}$ (dotted line) and large-time behavior given by Eq. (7) (dashed line) are also displayed, with P denoting the crossover point. The scaling of the spatial, temporal, and velocity variables is described in the text.

that the asymptote is an excellent approximation past the crossover point P.

The corresponding asymptote for the velocity of the front has the remarkable property that, when expressed in scaled variables and in terms of the position of the front, it becomes independent even of the initial concentration c_0,

$$\frac{L}{D}v_f = \frac{\pi}{2}\cot\frac{\pi}{2}\left(1-\frac{x_n}{L}\right). \quad (7)$$

The above expression is displayed in the lower panel of Fig. 1 and one notices again that the approximation is very good past the crossover point.

IV. RESULTS

The coupled nonautonomous CH (1) and guiding field (2) equations have been solved numerically for different values of the initial density c_0, diffusion constant D, and length L of

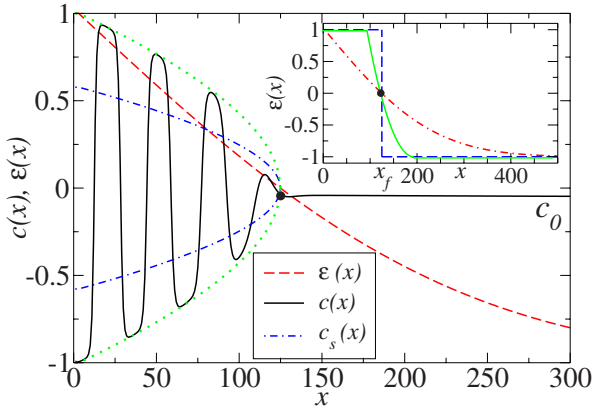

FIG. 2. (Color online) Early stage of pattern formation: snapshots of the concentration field $c(x)$ (continuous line), guiding field $\varepsilon(x)$ (dashed line), and spinodal lines $\pm\sqrt{\varepsilon(x)/3}$ (dash-dotted line). Dotted lines indicate the local equilibria $\pm\sqrt{\varepsilon(x)}$. The big dot represents the position of the instability front. The parameters are $c_0=-0.05$, $L=1000$, $D=4$, and $t=4000$. The inset shows various possible profiles of the guiding field (see Sec. VI), namely, the usual diffusive configuration (dash-dotted line), a steplike profile (dashed line), and a rigid parabola (continuous line).

the tube. Figure 2 illustrates the early stages of the cooling process, with the profiles of the concentration $c(x)$, guiding field $\varepsilon(x)$, and spinodal line $\pm c_s(x)=\pm\sqrt{\varepsilon(x)/3}$ at a given time $t<t_{\max}$ (before the instability front reaches the end of the tube). The concentration field inside the high- and low-density emerging bands relaxes rather rapidly to the instantaneous, local equilibrium values $\pm\sqrt{\varepsilon(x,t)}$, respectively.

The pattern initiated by the instability front evolves afterward till reaching a stationary profile, made of alternate regions of $c=\pm 1$ and rather sharp interfaces between them, throughout the whole tube. Strictly speaking, this "stationary" profile is still evolving through coarsening and band coalescence, as predicted, e.g., in [36]. However (except eventually for some very closely spaced bands; see below the comments on the plug), its characteristic evolution time is usually well beyond any reasonable experimental time [37]; from a practical point of view one can therefore safely assume its stationarity.

Three typical stationary patterns of the C-particle concentration field are represented in Fig. 3.

Before going into a more detailed analysis, let us enumerate some general qualitative features of the emerging patterns.

(i) The total number of bands increases as D increases, for fixed c_0 and L.

(ii) For fixed D and L, however, the number of bands decreases with increasing $|c_0|$ (approaching the spinodal).

(iii) The first part of the pattern displays regular banding (i.e., increasing distance between consecutive bands), while the second part displays inverse banding. It is important to note that the transition from one type of pattern to the other is related to the change in the behavior of the velocity of the guiding field, namely, from the initial diffusivelike motion to the later-time accelerated one (see Fig. 1).

(iv) In some situations, the pattern contains an initial plug, i.e., a rather wide initial region of constant concentration;

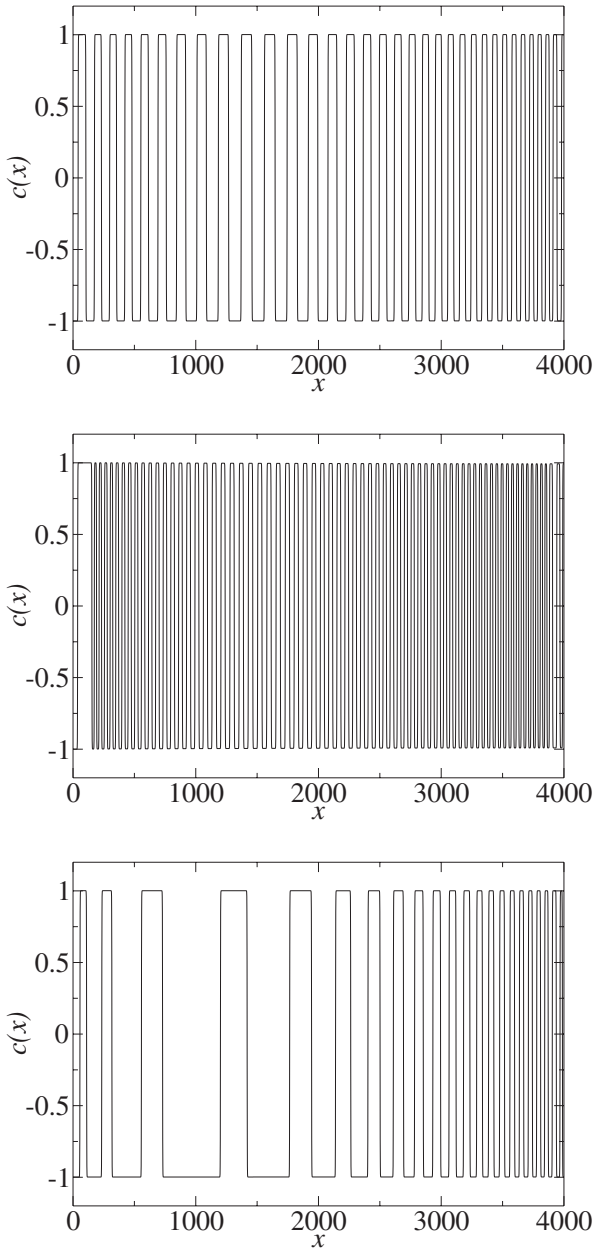

FIG. 3. Numerical solution $c(x)$ of the nonautonomous Cahn-Hilliard equation (1) in the long-time limit $t\gg t_{\max}$, and for system size $L=4000$. Top panel: $c_0=-0.05$ and $D=1$; middle panel: $c_0=-0.05$ and $D=8$; and bottom panel: $c_0=-0.2$ and $D=1$.

see, e.g., the second panel of Fig. 3. This effect has already been encountered in the usual Liesegang-pattern formation [10,11]. The plug may sometimes result from the coalescence, on a time scale of the order $O(t_{\max})$, of a certain number of very closely spaced bands [37]. A plug can also form at the end of the pattern, where the bands can again be close enough to each other. In contrast to the standard Liesegang pattern, whose spatial extension is limited only by the length of the tube, in our case the length of the patterned region can thus be limited by this band-coalescence effect.

Let us consider now the characteristics of the patterns from a more quantitative perspective. Figure 4 shows a plot

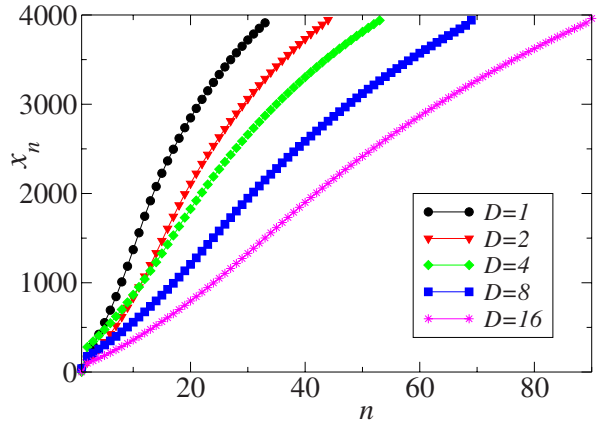

FIG. 4. (Color online) Position x_n of the nth band with respect to its label n for $c_0=-0.05$, $L=4000$, and different values of D.

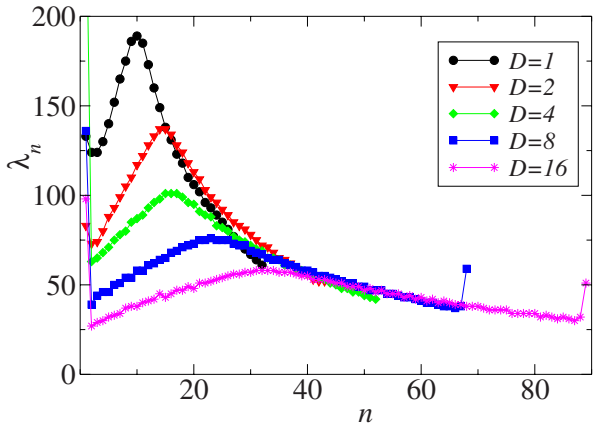

FIG. 5. (Color online) Distance $\lambda_n=x_{n+1}-x_n$ between two successive bands as a function of n, for $c_0=-0.05$, $L=4000$, and different values of D. One can notice outlier points at the beginning and ends of the curves. They correspond to the initial and final plug regions.

of the band positions x_n [which are taken, conventionally, to be the points where $c=0$, with an ascendent slope, $dc(x_n)/dx>0$, and are enumerated in the order of their appearance, starting from the $x=0$ end of the tube] as a function of n; different values of the diffusion constant D were considered, for fixed $c_0=-0.05$ and $L=4000$. The presence of a large initial plug may have some important effects on the n dependence of x_n for small n values. Accordingly, a simple and experimentally measurable functional expression is expected only for sufficiently large values of n, precisely as in the case of the usual Liesegang patterns.

For the initial, regular-banding part of the pattern, if enough bands are present, one can fit the positions of the bands reasonably well with a geometric series, $x_n\sim\exp(n\tilde{p})$, as for a standard Liesegang pattern [10,11]. This is obviously related to the initial diffusivelike motion of the instability front, which does not differ qualitatively from the motion of the reaction front in the usual Liesegang configuration [12]. However, a power-law fitting cannot be excluded either, and further detailed work meant to clarify this point is in progress and will be presented elsewhere.

For the second, inverse-banding part of the pattern, the positions of the bands for large n's can be fitted equally well as $x_n\sim\ln n$ or with a power law $x_n\sim n^{\beta}$, where the exponent $\beta\approx 0.2$–0.3 is practically independent of D. Since the corresponding distance $\lambda_n=x_{n+1}-x_n$ between consecutive bands behaves like $\lambda_n\sim n^{\beta-1}$, the inequality $\beta<1$ ensures precisely the inverse-banding character of the pattern.

Figure 5 displays $\lambda_n=x_{n+1}-x_n$ as a function of n, for the same parameter values as in Fig. 4. One notices clearly the initial region of regular banding (with the eventual spurious initial plug) and the inverse banding, with the final plug. The tails of these plots for large-n values do not allow to discriminate further between the two above-suggested fittings of the relation between x_n and n in the inverse-banding region.

Finally, in Fig. 6 we plot the width w_n of the nth high-density band as a function of n. It is remarkable that, except for a crossover region between direct and inverse banding, one can fit throughout, with a good approximation,

$$w_n \approx Wx_n + U. \tag{8}$$

For the regular-banding region $W>0$, and one can easily justify this result simply by using mass-conservation arguments for the C particles, as well as the geometric progression of band positions (see [10,11]). However, for the inverse-banding region $W<0$, and the approximate nature of this relationship is related to the fact that the band positions are not well fitted by a geometric series in this case. On this figure one can clearly see that, as already stated above, the transition from regular to inverse banding is marked by the crossover point P of the motion of the instability front, see Sec. III.

V. THEORETICAL ARGUMENTS

Our goal is to devise a simple theoretical approach able to explain the characteristics of the patterns observed in the numerical simulation of the nonautonomous CH equation (1), and to be used further on for predictive purposes. A basic

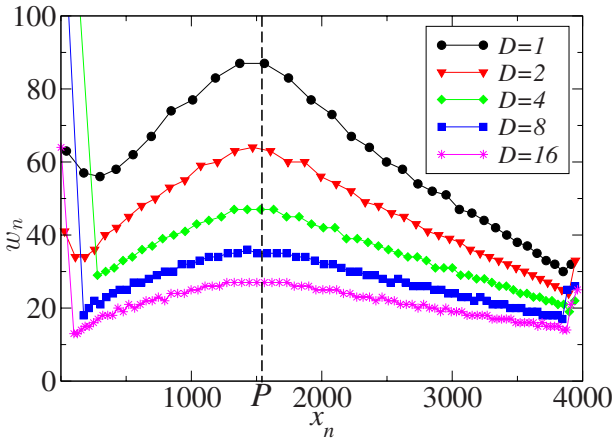

FIG. 6. (Color online) Width w_n of the nth band as a function of the band position x_n, for $c_0=-0.05$, $L=4000$, and different values of D. The vertical dashed line indicates the position of the crossover point P (see Sec. III). The jumps at the end points of the curves are due to the plugs.

element of our approach is the numerical finding that the characteristics of the patterns are directly related to the motion of the instability front. In particular, the local wavelength of the pattern $\lambda_n = x_{n+1} - x_n$ (see Figs. 5 and 6) is related to the velocity $v_f = v_f(x_f)$ of the front (see the second panel of Fig. 1), as discussed below.

Our approach is based on several assumptions, the validity of which is verified *a posteriori* by comparison of the theoretical findings with the results of the numerical simulations. Our first hypothesis is that the guiding field moves faster than the diffusing C particles; therefore, the phase separation does not take place ahead of the instability front, but only behind it. Note, however, that the velocity of the front should not be too high either, since otherwise our second hypothesis about the quasistationarity may not be satisfied. The meaning of the second hypothesis is that, although the local value of the spinodal concentration $c_s(x,t) = \sqrt{\varepsilon(x,t)/3}$ evolves in time in the wake of the instability front, this evolution can be assumed to be slow enough so that the local instability boundaries associated with the spinodal curve are in a quasistationary state. We assume therefore that the onset of the phase separation instability is pulled by the motion of the guiding front, and consequently we can use the standard results of the pulled-front theory [38–40] to establish the characteristics of the emerging pattern.

Let us recall here the main results of the standard theory. Consider an autonomous CH equation (1) with ε constant throughout the system, and a uniform unstable concentration c_0, $|c_0| < c_s = \sqrt{\varepsilon/3}$. A sharply localized perturbation of this state will then evolve into an instability front, with a well-defined velocity, leading to phase separation behind it and to the appearance of a pattern of well-defined wavelength. Using linear stability analysis arguments, one can easily compute both the wavelength λ^* of the most unstable mode and the asymptotic velocity v^* of the instability front as a function of the distance between the initial concentration and the spinodal value; namely,

$$\lambda^* = \frac{16\pi\sqrt{2}(\sqrt{7}+2)}{3(\sqrt{7}+3)^{3/2}} a^{-1/2}, \tag{9}$$

$$v^* = \frac{2(\sqrt{7}+2)}{3(\sqrt{7}+1)^{1/2}} a^{3/2}, \tag{10}$$

where $a \equiv 3(c_s^2 - c_0^2) = \varepsilon - 3c_0^2$. Except for the cases when one has band coalescence (coarsening), this wavelength provides the wavelength of the asymptotic emerging pattern. By eliminating the parameter a between these two expressions, one obtains a direct relationship between the asymptotic wavelength of the pattern and the asymptotic velocity of the instability front,

$$\lambda^* = \frac{9.642}{(v^*)^{1/3}}. \tag{11}$$

Note, however, that the relaxation of the system to this asymptotic state goes rather slowly, like $(1/t)$, both for the wavelength of the pattern and for the velocity of the instability front. Moreover, the transient effects tend to increase the wavelength of the pattern above its asymptotic value λ^* (see [38–40] for further details).

Using the above results of the pulled-front theory, we now make the ansatz that the relationship (11) remains valid for our nonautonomous CH equation. More precisely, we assume that the local wavelength of the pattern is determined by the instantaneous or local velocity of the instability front as

$$\lambda_n \approx \frac{9.642}{[v_f(x_n)]^{1/3}}. \tag{12}$$

The physical picture underlying the above assumption is the following. The instantaneous pulled-front velocity $v^* = v_f(t)$ dictates [see Eq. (10)] an instantaneous value of the parameter a; let us call it $a_f(t)$. This means that the local concentration in the vicinity of the quasistationary instability front adjusts rapidly to the value $c_f(t)$ corresponding to the parameter $a_f(t)$, namely, $a_f(t) = \varepsilon(x = x_f(t), t) - 3c_f^2(t)$.

The comparison of the theoretical findings based on the above ansatz with the results of the numerical simulations is displayed in Fig. 7, where the local wavelength of the pattern λ_n is plotted versus x_n for different values of D and L. This figure provides a double check of the ansatz.

(i) If Eq. (12) is valid, then, since $v_f(x_n)$ is universal under appropriate scaling of space, time, and velocities (according to Sec. III), the plots from the numerical results should merge when applying the rescaling $\lambda_n \to \lambda_n (D/L)^{1/3}$ and $x_n \to x_n/L$. This is, indeed, the case, as illustrated by both panels of Fig. 7.

(ii) All the rescaled plots should fit the theoretical formula (12) shown by solid lines in Fig. 7.

The agreement between our simple theoretical predictions and the results of the simulations is surprisingly good. The only exceptions are a few outlier points corresponding, respectively, to the early band formation (initial plug) and to the last bands close to the boundary (final plug). There is also a systematic initial and final mismatch, which may be due to the high acceleration of the instability front at the very beginning and the very end of its motion along the tube (see Fig. 1), and thus to the breaking of the quasistationarity hypothesis that lies at the basis of our ansatz. Another origin of discrepancy might be the dynamics of the guiding field profile, which may, under some circumstances, fail to satisfy the quasistationarity hypothesis.

We note that the agreement between numerics and theory is better for large values of the velocity of the instability front, i.e., for smaller values of L/D, as shown in the upper panel of Fig. 7 as compared to the lower panel. This is probably related to a better, respectively worse, adequacy of the basic hypothesis of a fast-moving front as compared to the diffusion of the C particles. Finally, the fact that the numerical wavelengths are systematically larger that the theoretically estimated ones may be due to the combined effect of slow relaxation to the asymptotic state and the quasistationary nature of our configuration during the onset of the pattern (see the comments above on the effects of transients on the wavelength, in the autonomous case).

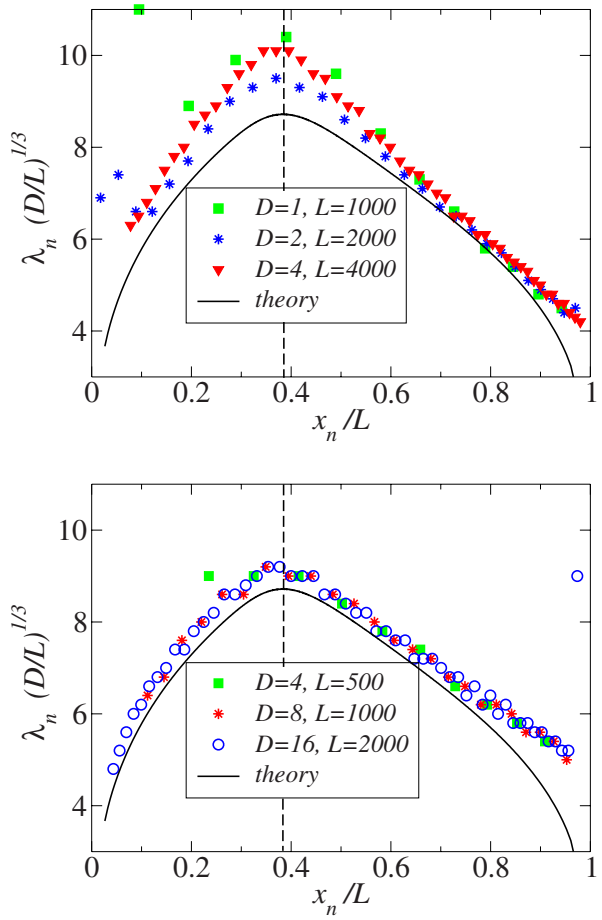

FIG. 7. (Color online) Comparison of the local wavelengths of the pattern as determined from numerical simulations (symbols) with the theoretical results based on Eq. (12) (continuous line). The wavelengths λ_n and the band positions x_n are rescaled as discussed in the text. Upper panel: $c_0=-0.05$ and $L/D=1000$. Lower panel: $c_0=-0.05$ and $L/D=125$. The vertical dashed lines indicate the position of the crossover point P where the instability front has a minimal velocity (see Sec. III). The outlier end points are due to the plugs.

VI. PATTERN CONTROL

We address now the problem of controllability of the characteristics of the emerging pattern. It is obvious from the above results that both the qualitative (i.e., regular or inverse banding) and quantitative (like total length of the pattern, pattern local wavelength, width of bands, etc.) features can be controlled in the described configuration through an appropriate choice of the parameters L, c_0, and (to a less extent, as more difficult to manipulate) D. Moreover, these results can be described theoretically in the frame of the pulled-front approximation thus providing a method for estimating the parameters of the patterns. However, this method of control, although very simple, is somewhat rigid, since the above-mentioned control parameters cannot be changed during the process, while, ideally, one requires an easily tuned, flexible, external tool of control. One can then think about moving the tube with the gel (or maybe a thin film of gel) in a prescribed temperature profile, with a velocity that can be changed at any moment according to need. One achieves therefore a guiding field $\varepsilon(x,t)$ that can be externally tuned at any moment and point.

For example, the simplest configuration one can imagine is an abrupt, steplike temperature profile that moves with velocity v_f, such that $\varepsilon(x,t)=-1+2\Theta(x-x_f(t))$ $(0\leqslant x\leqslant L)$, where $\Theta(\,)$ designates the Heaviside step function and $x_f(t)$ is the instantaneous position of the step. If the motion is uniform $v_f=$const, then one obtains equidistant banding. If the motion of the step is accelerated (decelerated) then the pattern presents inverse banding (regular banding), with characteristics that depend on the details of $v_f=v_f(t)$.

Another simple option is to propagate a smooth, given temperature profile along the tube, such that $\varepsilon(x,t)=F(x-x_f(t))$. Now, the characteristics of the emerging pattern depend not only on the velocity $v_f(t)$ of the propagating rigid guiding field profile, but also on the shape of this profile.

In order to illustrate these points, we considered, for comparison, the emerging pattern in three situations (also illustrated in Fig. 2):

(i) The diffusive guiding-field profile, as discussed in the previous sections, for a given set of parameters D, L, and c_0. Recall that the instability front moves with a velocity $v_f(t)$ described in Sec. III.

(ii) A steplike profile of the guiding field that moves with the same velocity $v_f(t)$.

(iii) Finally, a parabolic profile of the guiding field, $\varepsilon(x,t)=\{-1+\mathcal{A}[x_f(t)-x-x_0]^2\Theta(x_f(t)-x-x_0)\}$. One has $\varepsilon=-1$ for $x=x_f+x_0$ and the parameter $\mathcal{A}$ is determined such that for $x=x_f$ one has $\varepsilon=1-3c_0^2$. As before, this rigid profile moves with the same velocity $v_f(t)$.

The results of the numerical simulation are represented in Fig. 8, together with the theoretical result based on our ansatz. One can notice the following:

(i) The pattern can be effectively controlled by the proposed methods. The effects are qualitatively the same as for our usual configuration, but these new methods allow for more flexible control.

(ii) The pattern obtained for the paraboliclike profile (with $x_0=70$) is closer to the pattern obtained for our usual configuration, as well as to the theoretical predictions based on the pulled-front approximation; the pattern obtained for the steplike profile is much different. This convincingly illustrates the importance of the quasistationarity hypothesis for the pulled-front theory. Indeed, this basic ingredient is a good approximation both for our usual configuration and for the parabolic profile, but it is definitely absent in the case of the steplike profile, for which the associated abrupt jump in the local value of ε forbids any possibility of quasistationarity.

VII. CONCLUSION

We have discussed the problem of how to control precipitation patterns by bringing a system described by the Cahn-Hilliard equation into an unstable state using a prescribed guiding field. It was shown that a simple, physically realiz-

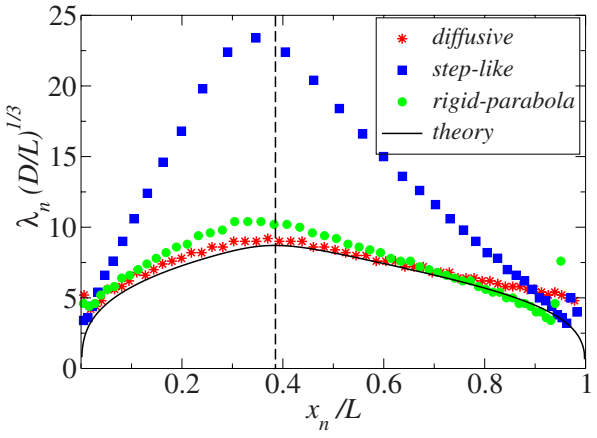

FIG. 8. (Color online) Local wavelengths of the pattern λ_n versus band positions x_n, in appropriately rescaled variables. Symbols: numerical simulations for three different profiles of the guiding field (see the text). Continuous line: theoretical calculations based on Eq. (12). The parameters are $c_0=-0.05$, $D=16$, and $L=2000$. The vertical dashed line indicates the position, along the cylinder's axis, of the crossover point P where the instability front has a minimal velocity (see Sec. III). The outliers at the beginning and end of the lines correspond to the plugs.

able field, such as a temperature field generated by a temperature jump at the boundary, is sufficient to generate rather complex precipitation patterns even in one dimension. The spacing characteristics of the patterns were determined numerically for the case of a diffusive guiding field, and we developed a quantitative theory for explaining the simulation results. The theory is based on relating the velocity of the instability front generated by the guiding field to the natural, pulled-front velocity of the phase-separation process which, in turn, controls the length scale of the pattern left in the wake of the moving front.

From a theoretical point of view, our results suggest that the inverse-banding phenomena observed in some Liesegang experiments may have an explanation in terms of a diffusive guiding field. This guiding field is perhaps not a temperature field, but may be generated by the diffusion of some chemical species which do not take part in the reactions and the precipitation but may change, e.g., the local pH value and thus influence the precipitation thresholds.

As far as technological applications are concerned, it appears that the problem of microfabrication of bulk structures by chemical reactions and precipitation [2–7] is just in the first stages of its development. The usefulness of this field will be decided on the possibility of creating flexible ways to ensure controllability. Our results suggest experimentally feasible solutions for the control of a particular precipitation process (formation of Liesegang bands). Clearly, further studies are necessary to develop new methods of control and to sort out the question of controllability in more complex cases.

ACKNOWLEDGMENTS

This research has been partly supported by the Swiss National Science Foundation and by the Hungarian Academy of Sciences (Grant No. OTKA T043734). Financial support is also acknowledged from the Program for Evolutionary Dynamics at Harvard University and NIH Grant No. R01GM078986 (T.A.).

[1] For a review, see M. C. Cross and P. C. Hohenberg, Rev. Mod. Phys. **65**, 851 (1994).
[2] For a recent review, see B. A. Grzybowski and C. J. Campbell, Mater. Today **10**, 38 (2007).
[3] M. Fialkowski *et al.*, J. Phys. Chem. B **110**, 2482 (2006).
[4] B. A. Grzybowski *et al.*, Soft Matter **1**, 114 (2005).
[5] M. Fialkowski, A. Bitner, and B. A. Grzybowski, Phys. Rev. Lett. **94**, 018303 (2005).
[6] M. I. Lebedeva, D. G. Vlachos, and M. Tsapatis, Ind. Eng. Chem. Res. **43**, 3073 (2004).
[7] O. Giraldo, Nature (London) **405**, 38 (2000).
[8] R. E. Liesegang, Naturwiss. Wochenschr. **11**, 353 (1896).
[9] H. K. Henisch, *Periodic Precipitation* (Pergamon, New York, 1991).
[10] Z. Rácz, Physica A **274**, 50 (1999).
[11] M. Droz, J. Stat. Phys. **101**, 509 (2000).
[12] T. Antal, M. Droz, J. Magnin, and Z. Rácz, Phys. Rev. Lett. **83**, 2880 (1999).
[13] Note that the reaction scheme can actually be rather complex. In particular, it can involve the possible existence of an intermediate compound; see, e.g., [14,15] for a more detailed discussion of these aspects and of related theoretical models.
[14] T. Antal, M. Droz, J. Magnin, Z. Rácz, and M. Zrinyi, J. Chem. Phys. **109**, 9479 (1998).
[15] M. Droz, J. Magnin, and M. Zrinyi, J. Chem. Phys. **110**, 9618 (1999).
[16] J. W. Cahn and J. E. Hilliard, J. Chem. Phys. **28**, 258 (1958).
[17] J. W. Cahn, Acta Metall. **9**, 795 (1961).
[18] P. C. Hohenberg and B. I. Halperin, Rev. Mod. Phys. **49**, 435 (1977).
[19] R. Matalon and A. Packter, J. Colloid Sci. **10**, 46 (1955); A. Packter, Kolloid-Z. **142**, 109 (1955).
[20] A. Toramaru, T. Harada, and T. Okamura, Physica D **183**, 133 (2003).
[21] I. Lagzi, Phys. Chem. Chem. Phys. **4**, 1268 (2002).
[22] M. Al-Ghoul and R. Sultan, J. Phys. Chem. A **107**, 1095 (2003).
[23] Z. Shreif, L. Mandalian, A. Abi-Haydar, and R. Sultan, Phys. Chem. Chem. Phys. **6**, 3461 (2004).
[24] I. Bena, F. Coppex, M. Droz, and Z. Rácz, J. Chem. Phys. **122**, 024512 (2005); I. Bena, M. Droz, and Z. Rácz, *ibid.* **122**, 204502 (2005).
[25] N. Kanniah, F. D. Gnanam, P. Ramasamy, and G. S. Laddha, J. Colloid Interface Sci. **80**, 369 (1980).
[26] P. Ortoleva, *Selected Topics from the Theory of Nonlinear Physico-Chemical Phenomena*, Theoretical Chemistry Vol. IV,

edited by H. Eyring (Academic, New York, 1978), pp. 236–288.

[27] J. Vollmer, G. K. Auernhammer, and D. Vollmer, Phys. Rev. Lett. **98**, 115701 (2007).

[28] E. L. Huston, J. W. Cahn, and J. E. Hilliard, Acta Metall. **14**, 1053 (1966).

[29] H. W. Alt and I. Pawlow, Physica D **59**, 389 (1992).

[30] P. Rebelo and G. V. Smirnov, J. Dyn. Control Syst. **11**, 413 (2005).

[31] For a review, see A. Bray, Adv. Phys. **43**, 357 (1994).

[32] The shift and rescaling of the concentration were done such that for the asymptotic state $\varepsilon=+1$ the stable uniform concentrations correspond to $c=\pm 1$. This can be achieved as

$$c = \frac{c(\text{unscaled}) - (c_h + c_l)/2}{(c_h - c_l)/2},$$

where $c_{h,l}$ denote, respectively, the unscaled high- and low-density equilibrium phase concentrations for $T=T_0$ $(\varepsilon=+1)$.

[33] An analogous configuration is obtained if one considers a new tube of length $2L$, cools it at both ends at T_0, and then concentrates on the behavior of only half of this new tube. Indeed, because of the symmetry with respect to the center of the new tube, there is no heat flux through its median section, which represents precisely the no-flux boundary condition in $x=L$.

[34] K. Binder and H. L. Frisch, Z. Phys. **84**, 403 (1991); X. Ye, J. Comput. Appl. Math. **150**, 87 (2003); R. Racke and S. Zheng (unpublished).

[35] J. Crank, *The Mathematics of Diffusion* (Oxford Science Publications, Oxford, 1975).

[36] J. S. Langer, Ann. Phys. (N.Y.) **63**, 53 (1971).

[37] S. Villain-Guillot, J. Phys. A **37**, 6929 (2004), and references therein.

[38] W. van Saarloos, Phys. Rep. **386**, 29 (2003).

[39] U. Ebert and W. van Saarloos, Phys. Rev. Lett. **80**, 1650 (1998).

[40] C. Storm, W. Spruijt, U. Ebert, and W. van Saarloos, Phys. Rev. E **61**, R6063 (2000).